THE JOURNAL OF CHEMICAL PHYSICS **122**, 054314 (2005)

Time-resolved intraband electronic relaxation dynamics of Hg_n^- clusters ($n=7-13,15,18$) excited at 1.0 eV

Arthur E. Bragg, Jan R. R. Verlet, and Aster Kammrath
Department of Chemistry, University of California, Berkeley, California 94720

Ori Cheshnovsky
School of Chemistry, The Sackler Faculty of Exact Sciences, Tel-Aviv University, 69978 Israel

Daniel M. Neumark[a]
Department of Chemistry, University of California, Berkeley, California 94720
and Chemical Sciences Division, Lawrence Berkeley National Laboratory, Berkeley, California 94720

(Received 17 September 2004; accepted 12 October 2004; published online 21 January 2005)

Time-resolved photoelectron imaging has been used to study the relaxation dynamics of small Hg_n^- clusters ($n=7-13,15,18$) following intraband electronic excitation at 1250 nm (1.0 eV). This study furthers our previous investigation of single electron, intraband relaxation dynamics in Hg_n^- clusters at 790 nm by exploring the dynamics of smaller clusters ($n=7-10$), as well as those of larger clusters ($n=11-13,15,18$) at a lower excitation energy. We measure relaxation time scales of 2–9 ps, two to three times faster than seen previously after 790 nm excitation of Hg_n^-, $n=11-18$. These results, along with size-dependent trends in the absorption cross-section and photoelectron angular distribution anisotropy, suggest significant evolution of the cluster anion electronic structure in the size range studied here. Furthermore, the smallest clusters studied here exhibit 35–45 cm^{-1} oscillations in pump-probe signal at earliest temporal delays that are interpreted as early coherent nuclear motion on the excited potential energy surfaces of these clusters. Evidence for evaporation of one or two Hg atoms is seen on a time scale of tens of picoseconds. © *2005 American Institute of Physics.* [DOI: 10.1063/1.1828042]

I. INTRODUCTION

Cluster science and nanoscience have been driven by a desire to understand the development of bulk properties correlated with the aggregation of material constituents, to elucidate the unique and unfamiliar properties of mesoscopic materials, and to develop new environments in which to study chemistry.[1,2] Consideration of quantum size effects on material properties and excited electron/charge-carrier dynamics is particularly crucial to the practical miniaturization of electronic and electro-optical devices. The development of metallic behavior in clusters of elemental metals has received considerable attention in this respect.[3] One means of probing the evolution of size-dependent metallic properties has been to investigate electronic relaxation dynamics in metal clusters spanning a very wide size-range, from nanoparticles[4–6] to very small elemental clusters.[7–9] Such experiments motivate the work presented here, in which we report further investigation of size-dependent electronic relaxation dynamics in mercury anion clusters, Hg_n^-, with the goal of understanding the subtle evolution of material behavior—specifically, electronic intraband relaxation dynamics—produced through clustering of divalent metal atoms.

In contrast to clusters composed of atoms of transition (e.g., Group 10) and simple metal (e.g., Groups 1 and 13) elements, which exhibit "metallic" behavior at relatively small sizes,[7,9–13] increased aggregation of divalent atoms (Groups 2 and 12) yields an intriguing development of material properties, resulting from the size-dependent interactions of the ns^2np^0 closed-shell atomic configurations.[1,14,15] Thus, inter-atomic interactions at small cluster sizes n are dominated by weak van der Waals (vdW) interactions common to clusters of rare gas atoms, while an increased degree of s-p hybridization, resulting from increased average coordination number at larger n, promotes covalent bonding character. At some size, clusters of divalent metal atoms exhibit metallic behavior with s-p band-gap (BG) closure, with which a metal-like Fermi level is obtained.[16,17] Thus, clusters below the critical size at which BG closure occurs are characteristically semiconductors.

Neutral mercury clusters have received particular attention both experimentally (spectroscopically) and theoretically regarding the size-dependent characteristics of divalent-metal clusters. Measurements of direct ionization[18,19] and autoionization[20] have been used to investigate subtle developments in ionization potential and absorption spectra with size, revealing marked changes in these properties at relatively small sizes ($n=13-20$). These experimental findings agree with a theoretically predicted "critical size regime" for the vdW-to-covalent bonding-type transition determined using a cluster tight-binding-type electronic structure model.[21] The nonmetal-to-metal transition in mercury clusters is expected to occur at even larger n and has been addressed most directly by Busani *et al.*,[16,22] who extrapolated a $6s$-$6p$ band-gap closure at $n \sim 400 \pm 50$ atoms from anion photo-

---

[a] Author to whom correspondence should be addressed. Fax: 510-642-3635. Electronic mail: dneumark@berkeley.edu

electron (PE) spectroscopy. Yet the dynamical consequences of such bonding-type transitions are relatively unexplored[23,24] and are of considerable experimental and theoretical interest.

Investigating anionic clusters has gained considerable appeal towards revealing the size-dependent evolution of material properties; the direct size selectivity inherent to negative ion experiments greatly facilitates tracing the evolution of cluster photophysics through stepwise aggregation. Coupling this size selectively with a ''universal'' time-resolved technique, such as time-resolved photoelectron spectroscopy (TRPES) or imaging (TRPEI),[25] permits direct investigation of cluster vibronic relaxation dynamics, as these techniques are sensitive to changes in cluster geometry and electronic structure. In the studies addressed here, the addition of an excess electron to clusters of divalent metals yields fundamentally *n*-doped semiconductor clusters ($6s^{2n}6p^1$) that exhibit pure electron-to-''phonon'' relaxation dynamics following excitation within the *p* band.

Our previous paper[26] [hereafter referred to as *I*] explored the one-color photodetachment of Hg_n^- clusters ($n=3-20$) using femtosecond laser pulses at 790, 395, and 263 nm. In addition, the time-resolved relaxation dynamics of Hg_n^- ($n=11-18$) were investigated with a 790–395 nm pump-probe TRPEI scheme, revealing ''slow'' relaxation time scales (generally, ~10 ps) following the initial near infrared, intraband $6p$ electronic excitation at $h\nu_{\mathrm{pu}}=1.57\,\mathrm{eV}$. These relaxation dynamics are broadly characterized by dispersive monotonic spectral shifts towards lower electron kinetic energy (alternatively, lower electronic energy within the $6p$ band) following excitation, and were modeled with a simple quasicontinuous kinetic relaxation cascade. The observed dynamics were attributed to sequential radiationless transitions between excited electronic levels occupied by the single unpaired $6p$ electron and are notably slower than the ultrafast multielectron relaxation dynamics observed following nonthermal excitation of transition metal cluster anions.[7,10–13]

In this paper, the work in *I* is extended using a lower pump photon energy of 1.0 eV. This allows comparison of the dynamics and relaxation rates of Hg_n^- clusters excited at different intraband excitation energies. Moreover, the pump-probe experiments can be extended to smaller clusters ($n=7-10$) for which the higher pump energy of 1.57 eV exceeds the photodetachment threshold.[16] We observe continuous binding energy shifts following excitation at 1.0 eV for all clusters studied, as seen for clusters $n>11$ at $E_{\mathrm{ex}}=1.57\,\mathrm{eV}$ in *I*, but with relaxation rates up to two to three times faster, on average, following excitation. A dramatic monotonic decrease in the resonant one- and two-color photodetachment signals with increasing cluster size is observed and is complemented by a noticeable evolution of $[1+1]$ photoelectron angular distribution (PAD) anisotropy over the same size range. We observe nuclear wave packet motion for the smallest clusters investigated here ($n=7,8$), identified from oscillations in time-dependent excited-state binding energy and signal intensity at early pump-probe delays, highlighting the coherent nuclear dynamics characteristic to early stages of the cluster relaxation dynamics upon intraband excitation. Finally, we find evidence for fragmentation as observed from photodetachment features observed at long pump-probe delays. These data, with that presented in *I*, are used to paint a comprehensive picture of the relaxation dynamics exhibited by mercury cluster anions within this size regime.

II. EXPERIMENT

The techniques used in this study are well documented in *I* and previous publications.[27–29] Briefly, anions are generated in a pulsed source, mass separated by time of flight, and are photoexcited and photodetached by femtosecond laser pulses. The resulting photoelectrons are then collected and analyzed with a collinear velocity-map imaging (VMI) electron optical system, yielding both electron kinetic energy (eKE) and PADs.

Hg_n clusters are generated by passing 40–50 psi (gauge) of Ar through a heated (210–235 °C) mercury reservoir in a 40 Hz high-temperature Even-Lavie pulsed valve.[30] The neutral beam intersects a pulsed electron beam, which generates cations and anions through collisional detachment and secondary electron attachment, respectively. The electrically neutral discharge passes through a pair of pulsed high-voltage electrodes, which inject anions into a Wiley-McLaren time-of-flight mass spectrometer[31] at ~1800 eV average kinetic energy. Adjacent cluster masses are easily separated within this range of cluster masses, though isotopic distributions remain unresolved.

Photoelectrons were collected using collinear anion VMI. Our implementation of this technique has been documented extensively elsewhere,[26–29] and is similar to that used by Sanov[32] and Bordas,[33] with the difference that photoelectrons are extracted collinearly, rather than perpendicularly, with respect to the parent ion beam. The VMI electron optical stack, based on the design of Eppink and Parker,[34] comprises three electrodes—repeller, extractor, and ground—that provide the cylindrically symmetric, inhomogeneous electric field required for a charged-particle immersion lens. The three-dimensional photoelectron velocity distribution generated in the laser interaction region, between the repeller and extractor electrodes, is projected onto a two dimensional (2D) position-sensitive detector. Optimal image focusing is obtained using a 70% extractor/repeller potential ratio. Phosphor emission from the detector is imaged with a Dalsa-1M30 charge coupled device (CCD) camera (Uniforce) at a 40 Hz repetition rate synchronized relative to ion production. The camera collects images in a 2×2 pixel binning mode (effectively, 512×512 pixels) in order to increase camera frequency and overall collection speed.

Pump and probe frequencies used in this experiment were generated from the 790 nm (1.57 eV), 1 mJ (500 Hz), 90 fs full width at half maximum chirped-pulse amplified output of a Ti:Sapphire femtosecond oscillator (Clark-MXR NJA-5, CPA-1000) through various frequency conversion schemes. Clusters were excited with the 1250 nm (1.0 eV, 20 μJ/pulse, 100 fs) signal output of an optically pumped generator/amplifier (TOPAS, light conversion); the excitation energy was determined from the measured wavelength of the second harmonic (SHG) of the OPA signal obtained with an Ocean Optics spectrometer. The 395 nm probe pulse (40–50

μJ, ~100 fs) was derived from second harmonic generation of the fundamental output. The IR pump pulse was delayed with respect to the fixed UV optical path length through use of a computer-controlled translation stage. The two beams were collinearly recombined and focused with a 50 cm lens to within the interaction region of the VMI lens. "Time zero" was determined from the pump-induced half-fall of direct UV (one-photon SH) photodetachment signal.

Data were typically acquired for 10 000–30 000 laser shots (100–200 s) at each pump-probe delay, typically resulting in the collection of 100 000–200 000 photoelectrons at each delay. Photoelectron spectra were normalized according to the integrated direct 395 nm and $[1+1']$ signal intensities. Normalization of two-color signal collected in different sets of scans was accomplished through image collection at a fixed delay relative to time zero. All images are four-way symmetrized to compensate for inhomogeneities in detector and CCD sensitivity. Three-dimensional velocity distributions were reconstructed using the basis set expansion (BASEX) forward convolution method developed by Dribinski *et al.*[35] Photoelectron kinetic energy distributions were obtained through velocity→energy transformation and radial integration of the $\phi=0$ slice of reconstructed, cylindrically symmetric 3D detachment distributions. We typically obtain a relative kinetic energy resolution $\Delta E/E$ of 5% following atomic anion photodetachment. PAD anisotropy parameters, $\beta_n(\epsilon)$, were acquired by fitting the 3D slice with an even series of Legendre polynomials $[P_n(\cos\theta)]$ appropriately truncated for an m photon photodetachment process ($n_{\max}=2m$);[36] see the Analysis for details.

III. RESULTS

Figure 1 outlines the cluster energetics and photoexcitation schemes relevant to the investigations reported here; detachment channels (lettered) and excitation/relaxation processes are explained below with reference to our observations. Figure 2 displays typical one-color photoelectron images, BASEX inversions, and PE spectra from photodetachment of Hg_7^- at (a) 395 nm and (b) 1250 nm. The laser polarization (symmetry axis) is vertical in this figure, as indicated. The photodetachment processes responsible for the features in Fig. 2 are the same as those outlined in *I*; the peak in Fig. 2(a) is from direct photodetachment at 395 nm [Fig. 1, *B*], while the peak in Fig. 2(b) is from $[1+1]$ resonant photodetachment at 1250 nm [Fig. 1, *A*]. Note that in contrast to *I*, where the probe photon energy was twice the pump energy, peaks in the PE spectra from processes *A* and *B* are not at the same eKE.

Figure 3 shows two-color PE spectra for Hg_n^- ($n=7-18,20$), measured within the pump-probe temporal overlap (0 ps); relevant photodetachment processes are labeled according to Fig. 1. These spectra were acquired with identical laser fluxes ($\sim 10^{11}$ W/cm^2) and have been normalized according to the intensities of the direct 395 nm photodetachment peaks (*B*). All detachment features shift monotonically to lower eKE with increasing size, though with a much steeper size dependence for smaller ($n=7-10$) relative to larger ($n=11-20$) clusters. Strikingly, the intensities of the $[1+1]$ and $[1+1']$ photodetachment features (Fig. 1, *A* and *C*, respectively) drop dramatically with increased cluster size. Size-dependent spectra exhibit direct and resonant two-color photodetachment features throughout the entire range of sizes studied. At larger cluster sizes, the low energy $[1+1]$ 1250 nm feature is obscured by a combination of 395 nm *interband* resonant $[1+1]$ photodetachment and Auger emission (Fig. 1, *D* and *E*, respectively); the former also contributes a weak photodetachment signal between the direct 395 nm and $[1+1']$ photodetachment peaks. As discussed in Sec. IV C, the reversal in dominance of the resonant and direct photodetachment features in these spectra indicates a dramatic reduction in cluster absorption cross-section at 1.0 eV with increasing size.

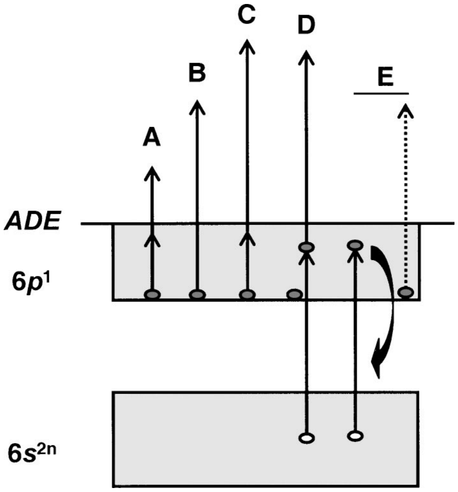

FIG. 1. Hg_n^- photoexcitation schemes/processes: (*A*) one-color, resonant two-photon photodetachment (R2PD) at 1250 nm; (*B*) direct UV (395 nm) photodetachment; (*C*) intraband two-color (1250+395 nm) R2PD (time-dependent); (*D*) UV resonant interband photodetachment; (*E*) UV interband excitation followed by electron-hole (e^--h^+) pair relaxation and recombination (curved line) with concomitant Auger electron emission (dotted arrow). The solid line, labeled *ADE*, signifies the adiabatic photodetachment threshold.

A temporal sequence of two-color pump-probe images and spectra is given in Fig. 4, illustrating the relaxation dynamics that follow 1250 nm intraband excitation of Hg_7^-. Image intensity is conveyed according to a logarithmic gray scale in order to highlight evolution of the $[1+1']$ feature. Each image (spectrum) contains three prominent features, which have been labeled in (a) according to Fig. 1. Starting from smallest radii (lowest energies), these are identified as the 1250 nm $[1+1]$ resonant one color (Fig. 1, *A*), the direct 395 nm (*B*), and the time-evolving $[1+1']$ resonant two-color (*C*) photodetachment signals. The 1250 nm $[1+1]$ photodetachment peak has been scaled in the photoelectron spectra in order to highlight the $[1+1']$ photodetachment dynamics (see Fig. 3 for comparison). As was observed at 790 nm, the initial electronic excitation yields a relatively isotropic $[1+1']$ photodetachment distribution $[\beta_2(t_0)\sim 0.2]$, which contracts with pump-probe delay. This is reflected in the photoelectron spectra as a photodetachment peak (*C*) that shifts with time from high to lower eKE.

Figure 5 shows time-dependent "waterfall" plots that illustrate the evolution of the PE spectra for Hg_7^- and Hg_{12}^-.

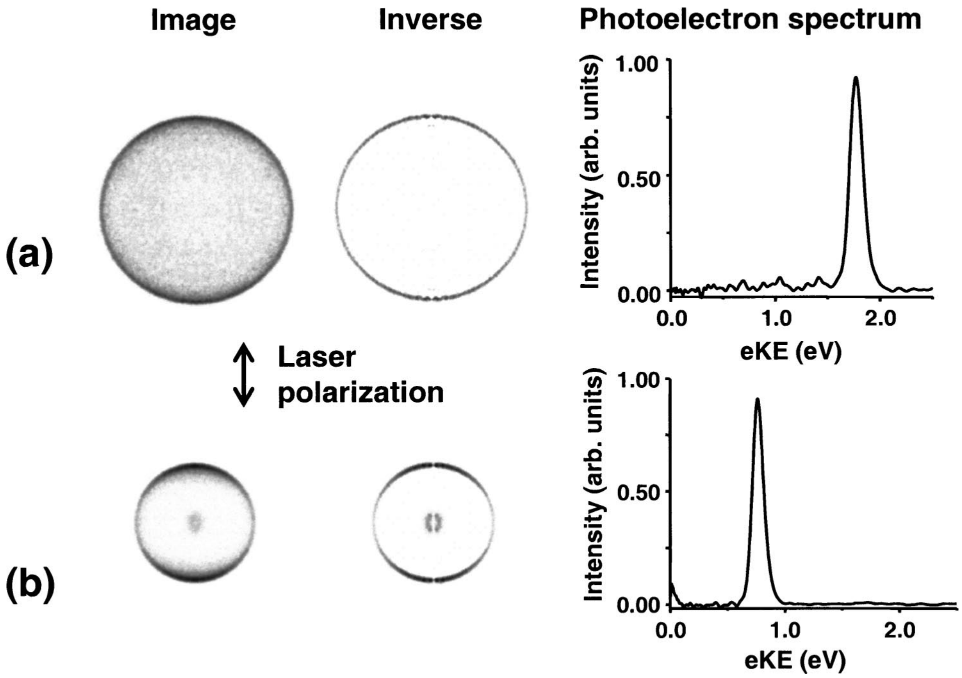

FIG. 2. One-color photodetachment of Hg_7^-: raw (but symmetrized) images, BASEX-inverted images, and photoelectron spectra. (a) direct 395 nm photodetachment; (b) 1250 nm intraband R2PD. Laser polarizations are vertical in the figure, as indicated.

These plots, and those for all other clusters studied at this pump energy, show the $[1+1']$ feature at high eKE continuously shifting with time toward lower eKE. For larger cluster sizes $(n \geqslant 10-11)$, where the probe energy surpasses the s-p band gap, there is some signal from interband resonant photodetachment (Fig. 1, *D*) in the same energy range as the $[1+1']$ feature, but the time dependence of the latter is still apparent. A series of photodetachment distributions collected at finer delays is given in Fig. 6 for $n=7$. The $[1+1']$ feature exhibits noticeable oscillatory behavior in kinetic energy with temporal delay. Similar but less dramatic behavior was observed in $n=8$, while oscillations were not apparent in the early-time TRPES of larger clusters.

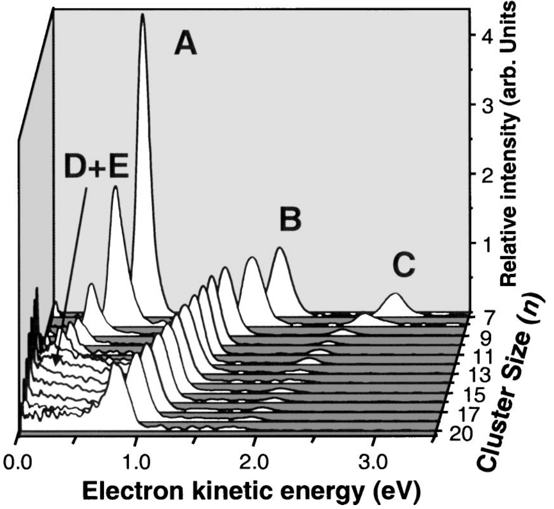

FIG. 3. Hg_n^- two-color (1250+395 nm) resonant photodetachment spectra collected at $\Delta t=0$ ps pump-probe delay for clusters $n=7-18$, 20. Spectra have been normalized according to the intensities of direct 395 nm photodetachment signal at each cluster size. Peaks are labeled according to the processes outlined in Fig. 1.

IV. ANALYSIS

A. Relaxation dynamics

The relaxation dynamics of Hg_n^- clusters following absorption at 1.0 eV are characterized by a continuous "cascade" to lower eKE. As discussed in *I*, this temporal evolution is attributed to a series of radiationless transitions between closely spaced electronic states of the singly occupied $6p$ band. While multiple time scales may be needed to model the overall relaxation dynamics, the decay rate of the initially prepared state is a useful first step in comparing cluster dynamics across size and excitation energy.

Briefly, initial relaxation time scales were determined through gated integration of time-dependent $[1+1']$ photodetachment signal present within the initial t_0 PE spectral window, i.e., the eKE range covered by this signal at the earliest times. As examples, the signal-integrated intensities for $n=7$ and 12 are plotted versus temporal pump-probe delay in Fig. 7. Time-dependent intensities were fit to single exponential decays,

$$I(t)=A_1 \exp(-t/\tau_n)+A_0, \tag{1}$$

at delays beyond the first few picoseconds, in order to avoid contributions from initial coherent signal contributions (c.f. $n=7$, 8). The decay time scales obtained are listed in Table I; relaxation rates are plotted in Fig. 8 against those measured in *I* at 1.57 eV. At $E_{\mathrm{ex}}=1.0$ eV, measured time scales drop by a factor of ~4 from between $n=7$ and 10 (8.94 and 2.28 ps, respectively), while leveling off to ~4.6 ps for $n=12$ and

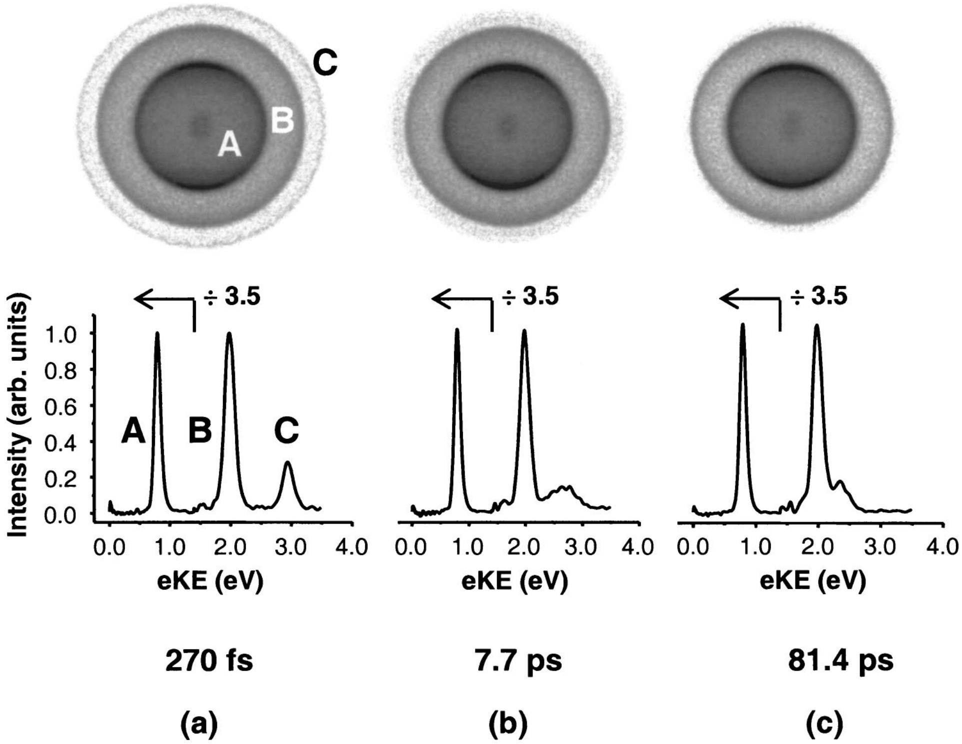

FIG. 4. Time-resolved photoelectron imaging of Hg_7^- dynamics probed at 395 nm following 1250 nm intraband absorption: symmetrized images and photoelectron spectra obtained at (a) 270 fs, (b) 7.7 ps, and (c) 81.4 ps pump-probe delays. The laser polarization is along the vertical direction of the page for all images.

higher. In all cases, the initial relaxation rates at 1.0 eV are substantially higher than at 1.57 eV, a somewhat unexpected result considered further in Sec. V.

B. Wave-packet motion

As seen in Fig. 6, the $[1+1']$ feature C for Hg_7^- oscillates at pump-probe delays between 0 and ~2 ps. The nature of these oscillations is shown more clearly in Fig. 9, where we have plotted the integrated signal in two adjacent eKE ranges (indicated in Fig. 6 with dashed lines). The maxima and minima of the oscillations in the two ranges are out of phase, indicative of vibrational wave packet motion in the initially excited state of the cluster anion. Similar results were obtained for Hg_8^-, although the amplitude of the oscillations was considerably smaller.

As wave packet coherence in these clusters is lost within a few cycles and is superimposed onto the dominant exponentially decaying contribution, oscillation frequencies were not obtained by Fourier transformation. Instead, they were determined from the peak-to-peak and trough-to-trough temporal separations, determined from the first derivative of the oscillating integrated signal intensity. Oscillations in $n=7$ photodetachment signal exhibit 700–800 fs peak-to-peak and trough-to-trough temporal spacings, with an average value of 750±40 fs and no clear increase with time. A temporal spacing of 900±100 fs was determined for the lower-amplitude oscillations seen in $n=8$. These temporal separations indicate coherence frequencies of 44±3 and 37±5 cm^{-1} for $n=7$ and 8, respectively. Additionally, the *total* time-evolving $[1+1']$ integrated intensity (Fig. 9, bottom) exhibits modulation at early delays for $n=7$.

C. Intraband absorption

The size-dependent two-color photodetachment spectra shown in Fig. 3 were used to investigate the intense intraband absorption observed in these clusters at near IR wavelengths. A general two-photon resonant photodetachment signal $S_{res}(n)$ is described by the simple mathematical relationship

$$S_{res}(n) \propto \sigma_{abs}[n;h\nu_1] I_1 \sigma_{\text{det}}[n;h\nu_2 - EA] I_2, \tag{2}$$

in which $\sigma_{abs}[n;h\nu_1]$ represents the size- and wavelength-specific absorption cross-section, $\sigma_{\text{det}}[n;h\nu_2-EA]$ represents the size- and eKE-dependent photodetachment cross-section, and I_m is the intensity for wavelength λ_m, where $m=1$ and 2 refer to the excitation and detachment wavelengths, respectively. As Hg_n^- photodetachment cross-sections are observed to be relatively constant >2–3 eV above threshold for a given cluster size, normalizing resonant signal to direct cluster photodetachment intensities,

$$S_{direct}(n) \propto \sigma_{\text{det}}[n;h\nu_2 - EA] I_2, \tag{3}$$

yields a quantity directly proportional to size-dependent absorption cross-sections ($\sigma_{abs}[n;h\nu_1] \propto S_{res}/S_{direct}$).

Figure 10 shows the relative size-dependent photodetachment intensities determined for both the resonant $[1+1]$ (solid squares) and $[1+1']$ (empty circles) features within the pump-probe temporal overlap, normalized to direct UV photodetachment intensities. Values for the $[1+1]$ and

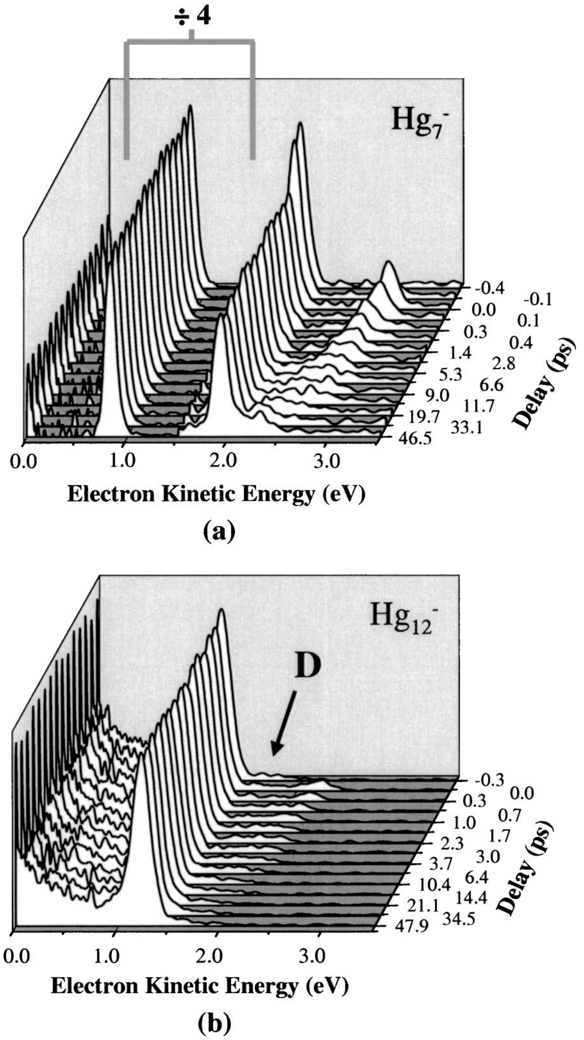

FIG. 5. TRPES "waterfall" progression of intraband relaxation dynamics: (a) Hg_7^-; (b) Hg_{12}^-. Resonant *interband* photodetachment (Fig. 1, process *D*) observed for $n > 11$ is labeled.

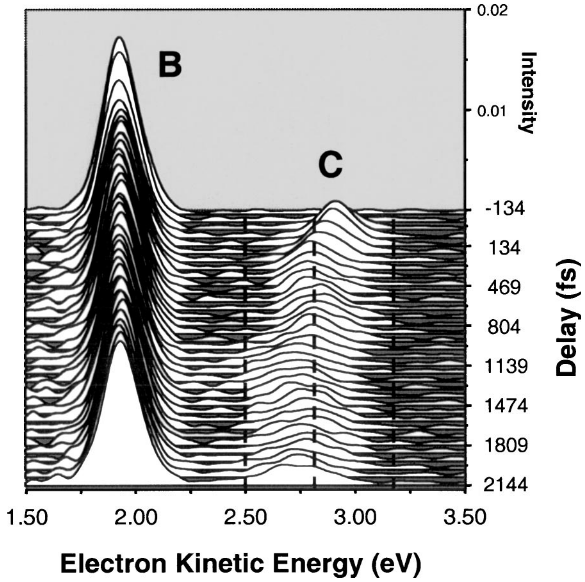

FIG. 6. Early-delay Hg_7^- relaxation dynamics. Dashed arrows indicate the gate-integrated and mutually out-of-phase spectral windows used to frequency-analyze signal oscillations (see Fig. 9).

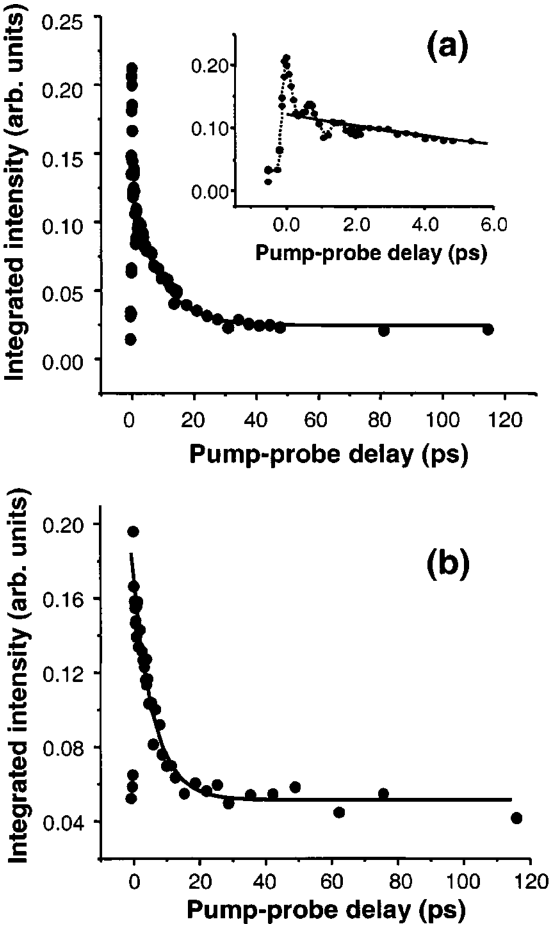

FIG. 7. Time-dependent integrated spectral intensities gated over the initial ($\Delta t = 0$ ps) two-color photodetachment features. (a) Hg_7^-; (b) Hg_{12}^-. Fitted single exponential decay curves (black) are overlaid and correspond to the time scales given in Table I. The inset of (a) shows early-delay single oscillations, which reflect nuclear wave packet motion.

$[1+1']$ intensities have been normalized according to their respective values at $n=7$ for purposes of comparison. Size dependence of the $[1+1]$ intensities could only be tracked to Hg_{12}^-, after which resonant interband photodetachment obscures resonant intraband photodetachment signal (see Fig. 3). The contribution to the $[1+1']$ signal from resonant interband photodetachment was estimated and subtracted. Error bars for both relative feature intensities were determined based on the reproducibility of intraband resonant relative to direct 395 nm photodetachment signal.

Figure 10 illustrates that $[1+1]$ and $[1+1']$ signal intensities measured within the temporal pulse overlap exhibit the same intensity reduction with cluster size. As these features are separated by ~2.15 eV, a range over which the photodetachment cross-section decreases dramatically, these virtually identical trends indicate a reduction in the intraband absorption cross-section at 1.0 eV with cluster size.

D. Photoelectron angular distributions

The 1250 nm $[1+1]$ PADs collected were fit to the standard expression,[36]

TABLE I. Hg_n^- intraband relaxation time scales measured following 1.0 eV photoexcitation.

Cluster size (n)	Relaxation time scale (ps)
7	8.94±0.88
8	4.85±0.46
9	2.89±0.25
10	2.28±0.22
11	3.20±0.49
12	4.63±0.51
13	4.70±0.22
15	4.49±0.29
18	4.59±0.32

$$I(\theta,\epsilon)\propto 1+\beta_2(\epsilon)P_2(\cos\theta)+\beta_4(\epsilon)P_4(\cos\theta), \qquad (4)$$

where $P_m(\cos\theta)$ represents the mth-order Legendre polynomial, θ is the polar angle between the photoelectron recoil vector and the laser polarization direction, and $\beta_m(\epsilon)$ corresponds to the mth PAD anisotropy parameter for photoelectrons generated with kinetic energy ϵ. Anisotropy parameters reported here represent average values over the full width of each [1+1] detachment feature. A central angular slice (~6°) was not included in the fitting, so as to eliminate contributions from the center-line noise introduced through inversion. The $\beta_m(\epsilon)$ values obtained for $n=7-12$ are given in Table II and are plotted in Fig. 11. Error bars were derived from duplicate measurements. The β_2 values determined drop dramatically over the reported range, dropping from ~0.7–0.8 for $n=7$, 8 to ~−0.2 for $n=11$, 12. Values of β_2 for photodetachment of clusters at 395 nm within this range of sizes were presented in *I*; these are also given in Table II and exhibit dramatic alteration in the same size regime. As PAD anisotropies are intimately correlated to the symmetry of the electronic orbital from which the electron is removed, these measurements provide evidence for variation in cluster electronic structure with increasing size and are discussed below in the context of size- and energy-dependent relaxation rates.

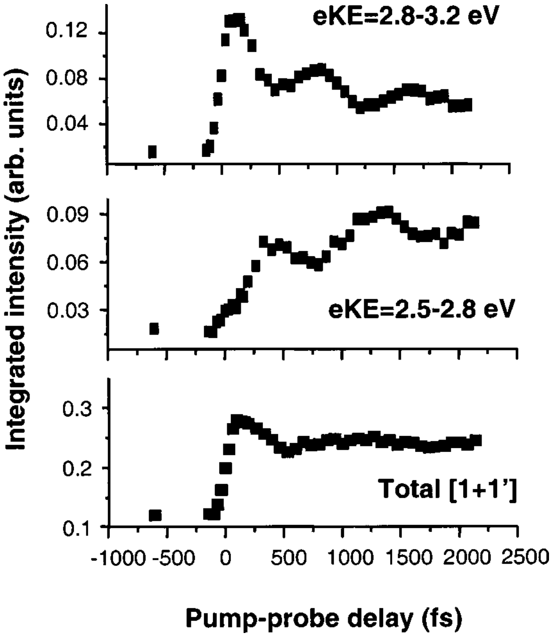

FIG. 9. Hg_7^- coherent nuclear motion, viewed from mutually out-of-phase signal contributions (top and middle; see Fig. 6) as well as *total* Hg_7^- [1+1′] intensity (bottom) at early pump-probe delays.

V. DISCUSSION

This investigation of the time-resolved relaxation dynamics of size-selected mercury cluster anions furthers the findings in *I* by examining cluster dynamics at a lower intraband excitation energy (1.0 eV). In addition to probing the effect of excitation energy on the clusters studied in *I*, we have studied smaller clusters ($n=7-10$) that undergo one-photon detachment at 1.57 eV, and are therefore unsuitable for pump-probe studies at that excitation energy. Finally, we have probed the evolution of cluster electronic structure by investigating [1+1] PAD anisotropies and relative cross-sections as a function of cluster size. The main size-dependent effects on dynamics, cross-section, and PAD anisotropy are shown in Figs. 8, 10, and 11, respectively. These

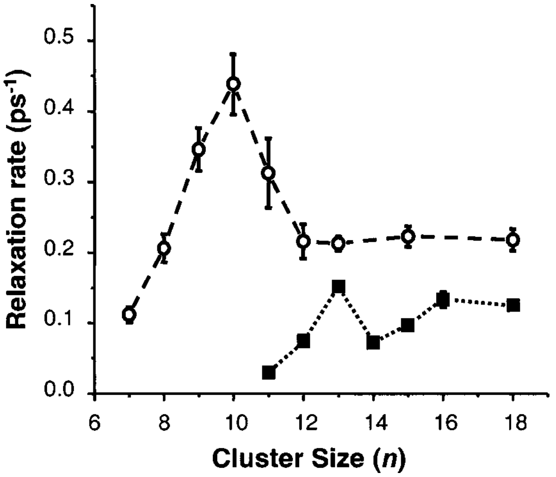

FIG. 8. Size-dependent intraband relaxation trends. Open circles −1.0 eV excitation; black squares −1.57 eV excitation, from *I*.

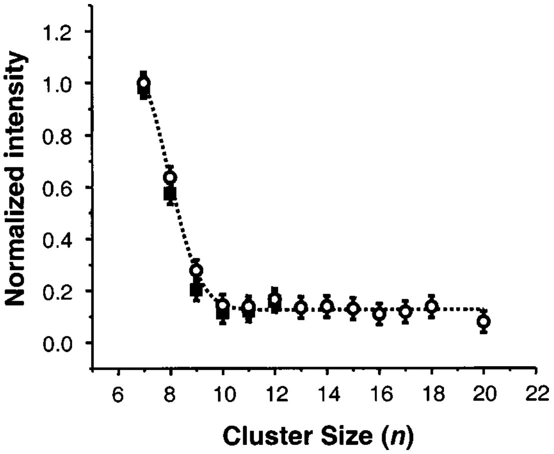

FIG. 10. Relative size-dependent signal intensities for one-color R2PD (solid squares) and two-color pump-probe ($\Delta t=0$ ps) photodetachment (empty circles). Normalization and error determination is described in the text. Dashed line—curve to guide the eye.

TABLE II. 1250 nm [1+1] resonant and 395 nm direct photodetachment PAD anisotropies. Fitting details and trends are discussed in the text; β_2 (395 nm) values were taken from *I*.

Cluster size (n)	β_2 (1250 nm)	β_4 (1250 nm)	β_2 (395 nm)
7	0.79 ±0.01	0.30±0.01	0.63
8	0.70 ±0.01	0.39±0.03	1.29
9	0.40 ±0.01	0.40±0.02	1.34
10	0.014±0.017	0.36±0.11	0.90
11	−0.044±0.01	0.26±0.01	0.63
12	−0.15 ±0.01	0.15±0.02	0.12

are discussed in more detail below, along with the implications of the coherent wave packet dynamics as evidenced by the results in Figs. 6 and 9.

A. General characteristics and dynamical trends

The time-dependent PE spectra in Fig. 5, in which photodetachment signal from the initially excited state smoothly shifts toward lower eKE over several picoseconds, are similar to those obtained for all clusters at 1.57 eV excluding Hg_{11}^-, for which the state initially excited at 1.57 eV behaves as a dynamical bottleneck.[26] However, as shown in Fig. 8, all clusters studied at both excitation energies exhibit markedly faster initial relaxation time scales at 1.0 eV. This result runs counter to trends in radiationless transition rates in molecules with relatively sparse manifolds of electronic states, where one usually observes faster relaxation with increasing excitation energy.[37] In such molecules, increased excitation energy corresponds to accessing higher vibrational levels of an excited electronic state, resulting in more favorable Franck-Condon factors for a radiationless transition to a lower-lying state. As discussed in *I*, Hg_n^- clusters do *not* have a sparse manifold of electronic states; the average level spacing in the p band is around 0.1 eV. The rates in Fig. 8 provide additional evidence of unusual trends in relaxation dynamics presumably resulting from this dense electronic level structure.

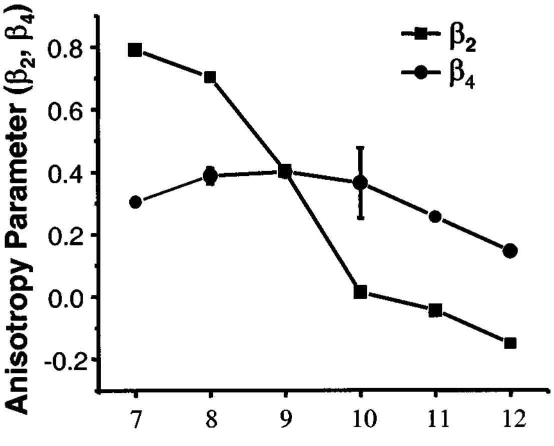

FIG. 11. Size-dependent ($n=7-12$) 1250 nm resonant photodetachment PAD anisotropy parameters (β_2,β_4).

We consider this issue further by reviewing the model used to describe the relaxation dynamics observed in *I*, in which population dynamics are mathematically expressed by

$$\frac{dN_i}{dt}=\sum_{j<i} k_{ji}N_j-\sum_{j>i} k_{ij}N_i . \tag{5}$$

Here, N_i is the population of level i and k_{ij} represents the internal conversion rate from level i to level j. The first term in Eq. (5) accounts for the population of level i from higher lying electronic levels, whereas the second term accounts for population transfer from i to lower-lying electronic states. Electronic relaxation is treated kinetically in this model, wherein state-to-state relaxation rates are scaled according to a simple energy-gap law, $k_{ij}=k\exp(-\Delta E_{ij})$; ΔE_{ij} is a scaled energy gap given by $\Delta E_{ij}=(j-i)\Delta E_{av}^{(n)}/\Delta E_{av}$, where $\Delta E_{av}^{(n)}$ is the average spacing between electronic states in neutral mercury clusters estimated from calculations by Pastor and Benneman,[38] and ΔE_{av} is an average anion level spacing (~10 states/eV) that recovers the characteristics of relaxation following 1.57 eV excitation, including time-dependent spreading of photoelectron distributions and a linear time dependent ⟨eKE⟩.

In terms of this model, state-dependent relaxation rates are determined by both the "local" electronic coupling strength, encoded in k_{ij}, and the electronic density of states (DOS), reflected in ΔE_{av}. Thus the differences in decay lifetimes at 1.0 and 1.57 eV may be considered in terms of variation of these two properties with excitation energy. In other words, at lower excitation energy, either the intraband couplings k_{ij} are larger, the DOS is larger, or both. No calculations on the coupling strength between electronic levels of the p band are available. However, Pastor and Benneman[38] have calculated the electronic energy levels of the $6p$ band for a wide range of neutral mercury clusters. They find these states to be distributed unevenly across the band; in most cases the DOSs are bimodal (c.f. Hg_6), with considerable level "bunching" at low (<~1 eV) and high energies (>~2 eV) in the band. Hence, the assumption of a uniform DOS assumed in our model is likely to be an oversimplification, and the more realistic bimodal DOS could account for the faster relaxation at 1.0 eV excitation energy.

The trends in relaxation rate with size at both excitation energies are also of considerable interest. Figure 8 shows that the cluster relaxation rates at 1.0 eV excitation increase by a factor of 4.5 as the cluster size increase from $n=7$ to 10, then drop by $n=12$ and remain constant for larger clusters. A similar pattern occurs at 1.57 eV, but is shifted to higher cluster sizes and lower overall rates. As discussed in *I*, these results cannot be explained as an electronic DOS effect, since the average DOS rises slowly and monotonically through the size range studied here.

At 1.0 eV, the $n=7-10$ size range, where the largest variation of relaxation rate occurs, is the same as that over which the intraband absorption cross-section (Fig. 10) and [1+1] PAD anisotropy (Fig. 11) exhibit the most variation. Measurement of all three aspects of the electronic structure and dynamics of these clusters thus indicates that we are still in the "small cluster" regime[2] where the addition of each atom brings about significant changes in the properties of the cluster. The size dependence of the cluster anion properties measured in this study drops considerably beyond $n=12$, while at 1.57 eV excitation energy the relaxation rates show considerable variation with cluster size up to $n=16$ (see Fig. 8). While the results at 1.57 eV might point toward a correspondence between strongly size-dependent properties with the predicted transition from van der Waals to covalent bonding in neutral Hg_n clusters in the range of 13–20 atoms,[20,21] the strong size dependence at 1.0 eV occurs within the neutral van der Waals regime. This somewhat counterintuitive result may be an indication that the evolution of bonding character in the anion clusters is quite different from that in the neutrals for the relatively small clusters studied here.

B. Early-delay dynamics

The signal oscillations observed at early times for $Hg_{7,8}^-$ are highly suggestive of cluster nuclear wave packet motion, whereby a few low-frequency vibrational modes are coherently populated in the initially excited state through excitation with the $\sim 150\ \mathrm{cm}^{-1}$ pump-pulse bandwidth. As the resulting wave packet oscillates, its vertical detachment energy varies, and the photoelectron spectrum at various eKEs probes different phases of the wave packet motion. This scenario is reminiscent of wave packet dynamics that are well-documented for Na_2,[39] I_2,[40] I_2^- (bare and clustered),[41,42] and Ag_4.[43] Somewhat more unusual is the periodicity in the integrated excited state signal at early times, seen in the bottom trace of Fig. 9, which indicates an overall time-dependent modulation in the excited state photodetachment cross-section associated with wave packet motion.

Regrettably, no supporting data is available regarding the vibrational frequencies of these anion clusters. However, Flad *et al.* have calculated the vibrational frequencies of small neutral clusters of divalent metal atoms using a variety of *ab initio* methods.[15] Small Hg_n $(n=3-6)$ clusters were determined to have average vibrational frequencies, $\overline{\omega}$, ranging 25–36 cm^{-1}; furthermore, these authors calculated a 37.4 cm^{-1} vibrational frequency for a bicapped tetrahedral Hg_6, as well as 40–50 cm^{-1} symmetric and degenerate frequencies for tetrahedral Hg_4 and trigonal bipyramidal Hg_5 structures. These calculated vibrational frequencies are certainly within the range of the experimental frequencies (35–45 cm^{-1}) for Hg_7^- and Hg_8^- obtained by analyzing our results as discussed in Sec. IV B.

As mentioned is Sec. IV B, oscillations at early time are most pronounced for Hg_7^-, much less evident for Hg_8^-, and not seen at all for the larger clusters. The observation of vibrational coherences requires that the lifetime of the initially excited state exceeds the vibrational period for the pump-activated mode(s), and that relatively few modes are excited. Hg_7^- is a favorable case because it has the longest lifetime of all the clusters studied here, and it may also have a highly symmetric pentagonal bipyramidal D_{5h} geometry in its ground and excited state,[44] resulting in a small number of active (totally symmetric) vibrational modes. While the structural details for the larger anions $(n>7)$ are unavailable, simply "capping" the lowest-energy $n=7$ anion and neutral structures with an additional atom already generates structures with more subtle geometry differences. Weaker coherences may be anticipated, consequently, due to a reduction in cluster symmetry and an increased number of participating symmetric vibrational modes. We note that at 1.57 eV, only Hg_{11}^-, the cluster with the longest excited state lifetime, showed any evidence for wave packet motion at early times.[26]

Finally, we point out that vibrational wave packet motion was observed by Bescos *et al.*[23] in a time-resolved study of neutral Hg clusters with as many as 60 atoms and was attributed to coherent excitation of a dimer-core embedded in a much larger cluster.[24] Such a mechanism is unlikely to apply in our experiment because we do not expect the intraband transitions excited in the anion experiments to be localized.

C. Long-time dynamics

It is evident from Figs. 4 and 5 that at the longest pump-probe delays in this experiment, the two-photon signal (process *C*) occurs at higher eKE than the probe-only signal (process *B*), signifying that the system has not returned to its original state. A similar effect was noted in *I* and attributed either to the spectrum being dominated by vibrational hot bands at long times, as a result of the vibrational heating that accompanies the electronic relaxation dynamics, or from evaporation of cluster atoms, which reduces the cluster vertical binding energy (VBE) and therefore results in signal at higher eKE. Arguments were presented favoring at least some evaporation occurring on the time scale of the experiment, but the definitive assignment of this long-time shift at 1.57 eV excitation to evaporation was complicated by the rather small VBE changes per atom for parent Hg_n^- clusters with $n \geqslant 11$. On the other hand, evaporation from the smaller clusters studied here should result in much larger decrements in the VBE; loss of one atom from Hg_7^-, for example, drops the VBE by 0.20 eV.[16]

Figure 12(a) shows long-time TRPE spectra for Hg_7^- spanning 14.2–47.8 ps. During this time, the pump-probe feature evolves into a single, broad peak separated from the probe-only PE peak by ~ 400 meV, roughly the energy difference between the $n=5$ and $n=7$ binding energies. This long time signal is directly compared to the direct 395 nm photodetachment signal of smaller clusters in Fig. 12(b). Probe-pump photodetachment signal has been subtracted from a long-time TRPES here and is given as a solid line; the pre-time-zero spectrum was scaled to 80% before subtraction, to eliminate subtraction-based spectral depletion. Direct $n=5$ and 6 photodetachment distributions are given as dashed and dotted lines, respectively. Clearly, the relaxed PE energy straddles the direct photodetachment features of the two smaller clusters, strongly suggesting that it results from daughter ions produced by evaporation of one or two Hg atoms from Hg_7^-. Thus, while most of the evolution of the TRPE spectra is from electronic relaxation, there does appear to be concomitant evaporation on the time scale of our measurements.

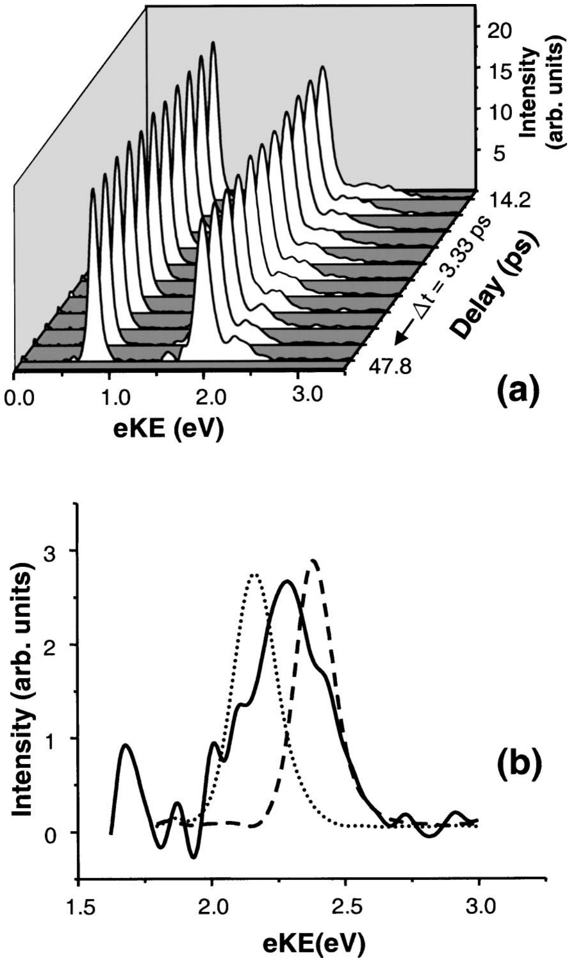

FIG. 12. Hg_7^- long-time TRPES: (a) dynamic progression at the end of the vibronic relaxation cascade; (b) long-time (47.8 ps) pump-probe signal (solid) compared to $n=5$ (dashed) and 6 (dotted) direct photodetachment spectra. The [1+1] R2PD feature is scaled as in Fig. 5. Relevance to fragmentation is considered in the Discussion.

VI. CONCLUSIONS

The intraband relaxation dynamics of Hg_n^- clusters ($n = 7-13,15,18$) have been investigated following excitation at 1.0 eV by time-resolved photoelectron imaging. Relaxation dynamics observed here are similar to those observed in our previous study following 1.57 eV excitation,[26] though exhibiting, on average, relaxation rates two to three times faster. Early-time oscillatory structure observed in the relaxation dynamics of $n=7$, 8 reflect the activation of nuclear wave packet motion ($\omega_{\mathrm{ave}}=35-45\,\mathrm{cm}^{-1}$) with or shortly following excitation, and highlights molecularity at smaller cluster sizes. Finally, analysis of size-dependent resonant intraband photodetachment intensities and PAD anisotropies offers insight regarding the electronic level structures involved in the cluster relaxation pathway.

These experiments establish a foundation for further investigating the size-and energy-dependent relaxation dynamics of these clusters, which will offer valuable benchmarks for cluster science. Furthermore, an understanding of the pure electronic-vibrational relaxation mechanism in these clusters is crucial to discriminating and possibly deconvolving competing processes in the electron-hole relaxation dynamics of interband excited clusters. We are pursuing both of these directions in our current research program.

ACKNOWLEDGMENTS

This research was supported by the National Science Foundation under Grant No. DMR-0139064 and by the U.S.-Israel Binational Science Foundation. A.K. was supported by the Abramson Graduate Fellowship in Chemistry.

[1] *Clusters of Atoms and Molecules. Theory, Experiment and Clusters of Atoms*, edited by H. Haberland (Springer, Berlin, 1994), Vol. 52.
[2] J. Jortner, Z. Phys. D: At., Mol. Clusters **24**, 247 (1992).
[3] R. L. Johnston, Philos. Trans. R. Soc. London, Ser. A **356**, 211 (1998).
[4] J.-Y. Bigot, J.-C. Merle, O. Cregut, and A. Daunois, Phys. Rev. Lett. **75**, 4702 (1995).
[5] J. H. Klein-Wiele, P. Simon, and H. G. Rubahn, Phys. Rev. Lett. **80**, 45 (1998).
[6] C. Voisin, D. Christofilos, N. Del Fatti *et al.*, Phys. Rev. Lett. **85**, 2200 (2000).
[7] N. Pontius, G. Lüttgens, P. S. Bechthold, M. Neeb, and W. Eberhardt, J. Chem. Phys. **115**, 10479 (2001).
[8] C. D. Grant, A. M. Schwartzberg, Y. Y. Yang, S. W. Chen, and J. Z. Zhang, Chem. Phys. Lett. **383**, 31 (2004).
[9] P. Gerhardt, M. Niemietz, Y. D. Kim, and G. Ganteför, Chem. Phys. Lett. **382**, 454 (2003).
[10] N. Pontius, P. S. Bechthold, M. Neeb, and W. Eberhardt, J. Electron Spectrosc. Relat. Phenom. **106**, 107 (2000).
[11] N. Pontius, P. S. Bechthold, M. Neeb, and W. Eberhardt, Phys. Rev. Lett. **84**, 1132 (2000).
[12] N. Pontius, P. S. Bechthold, M. Neeb, and W. Eberhardt, Appl. Phys. B: Lasers Opt. **B71**, 351 (2000).
[13] N. Pontius, M. Neeb, W. Eberhardt, G. Lüttgens, and P. S. Bechtold, Phys. Rev. B **67**, 035425 (2003).
[14] B. Hartke, Angew. Chem., Int. Ed. **41**, 1468 (2002).
[15] H.-J. Flad, F. Schautz, Y. Wang, M. Dolg, and A. Savin, Eur. Phys. J. D **6**, 243 (1999).
[16] R. Busani, M. Folkers, and O. Cheshnovsky, Phys. Rev. Lett. **81**, 3836 (1998).
[17] O. C. Thomas, W. J. Zheng, S. J. Xu, and K. H. Bowen, Phys. Rev. Lett. **89**, 213403 (2002).
[18] P. J. Harbour, J. Phys. B **4**, 528 (1970).
[19] K. Rademann, B. Kaiser, U. Even, and F. Hensel, Phys. Rev. Lett. **59**, 2319 (1987).
[20] C. Bréchignac, M. Broyer, P. Cahuzac, G. Delacretaz, P. Labastie, and L. Wöste, Chem. Phys. Lett. **120**, 559 (1985).
[21] M. E. Garcia, G. M. Pastor, and K. H. Bennemann, Phys. Rev. Lett. **67**, 1142 (1991).
[22] R. Busani, M. Folkers, and O. Cheshnovsky, Philos. Mag. B **79**, 1427 (1999).
[23] B. Bescós, B. Lang, J. Weiner, V. Weiss, E. Wiedenmann, and G. Gerber, Eur. Phys. J. D **9**, 399 (1999).
[24] W. Klaus, M. E. Garcia, and K. H. Bennemann, Z. Phys. D: At., Mol. Clusters **35**, 43 (1995).
[25] A. Stolow, A. E. Bragg, and D. M. Neumark, Chem. Rev. (Washington, D.C.) **104**, 1719 (2004).
[26] J. R. R. Verlet, A. E. Bragg, A. Kammrath, and D. M. Neumark, J. Chem. Phys. **121**, 10015 (2004).
[27] A. E. Bragg, R. Wester, A. V. Davis, A. Kammrath, and D. M. Neumark, Chem. Phys. Lett. **376**, 767 (2003).
[28] A. V. Davis, R. Wester, A. E. Bragg, and D. M. Neumark, J. Chem. Phys. **118**, 999 (2003).
[29] A. E. Bragg, J. R. R. Verlet, A. Kammrath, and D. M. Neumark, J. Chem. Phys. **121**, 3515 (2004).
[30] U. Even, J. Jortner, D. Noy, N. Lavie, and C. Cossart-Magos, J. Chem. Phys. **112**, 8068 (2000).
[31] W. C. Wiley and I. H. McLaren, Rev. Sci. Instrum. **26**, 1150 (1955).
[32] E. Surber and A. Sanov, J. Chem. Phys. **118**, 9192 (2003).
[33] C. Bordas, F. Paulig, H. Helm, and D. L. Huestis, Rev. Sci. Instrum. **67**, 2257 (1996).
[34] A. T. J. B. Eppink and D. H. Parker, Rev. Sci. Instrum. **68**, 3477 (1997).

[35] V. Dribinski, A. Ossadtchi, V. A. Mandelshtam, and H. Reisler, Rev. Sci. Instrum. **73**, 2634 (2002).
[36] K. L. Reid, Annu. Rev. Phys. Chem. **54**, 397 (2003).
[37] G. S. Beddard, G. R. Fleming, O. L. Gijzeman, and G. Porter, Chem. Phys. Lett. **18**, 481 (1973).
[38] G. M. Pastor and K. H. Bennemann, in *Clusters of Atoms and Molecules*, edited by H. Haberland (Springer, Berlin, 1994), pp. 86–113.
[39] A. Assion, M. Geisler, J. Helbing, V. Seyfried, and T. Baumert, Phys. Rev. A **54**, R4605 (1996).
[40] I. Fischer, M. J. J. Vrakking, D. M. Villeneuve, and A. Stolow, Chem. Phys. **207**, 331 (1996).
[41] A. V. Davis, R. Wester, A. E. Bragg, and D. M. Neumark, J. Chem. Phys. **119**, 2020 (2003).
[42] M. T. Zanni, A. V. Davis, C. Frischkorn, M. Elhanine, and D. M. Neumark, J. Chem. Phys. **112**, 8847 (2000).
[43] H. Hess, K. R. Asmis, T. Leisner, and L. Woste, Euro. Phys. J. D: At., Mol. Clusters **16**, 145 (2001).
[44] Y. Wang, H.-J. Flad, and M. Dolg, Int. J. Mass. Spectrom. **201**, 197 (2000).